



Article

Estimation of Apple Flowering Frost Loss for Fruit Yield Based on Gridded Meteorological and Remote Sensing Data in Luochuan, Shaanxi Province, China

Yaohui Zhu ^{1,2,3} , Guijun Yang ^{2,3}, Hao Yang ^{2,3}, Fa Zhao ^{2,3}, Shaoyu Han ^{2,3}, Riqiang Chen ^{2,3}, Chengjian Zhang ^{2,3}, Xiaodong Yang ^{2,3}, Miao Liu ^{2,3}, Jinpeng Cheng ^{1,2,3} and Chunjiang Zhao ^{1,2,3,*}

¹ School of Information Science and Technology, Beijing Forestry University, Beijing 100083, China; yaohui_zhu@bjfu.edu.cn (Y.Z.); niceget@bjfu.edu.cn (J.C.)

² Key Laboratory of Quantitative Remote Sensing in Agriculture of Ministry of Agriculture, Beijing Research Center for Information Technology in Agriculture, Beijing 100097, China; yanggj@nercita.org.cn (G.Y.); yangh@nercita.org.cn (H.Y.); p18101005@stu.ahu.edu.cn (F.Z.); 13598834331@stu.henau.edu.cn (S.H.); 211804020006@home.hpu.edu.cn (R.C.); 18210210075@stu.xust.edu.cn (C.Z.); yangxd@nercita.org.cn (X.Y.); 19210010011@stu.xust.edu.cn (M.L.)

³ National Engineering Research Center for Information Technology in Agriculture, Beijing 100097, China

* Correspondence: zhaojc@nercita.org.cn



Citation: Zhu, Y.; Yang, G.; Yang, H.; Zhao, F.; Han, S.; Chen, R.; Zhang, C.; Yang, X.; Liu, M.; Cheng, J.; et al. Estimation of Apple Flowering Frost Loss for Fruit Yield Based on Gridded Meteorological and Remote Sensing Data in Luochuan, Shaanxi Province, China. *Remote Sens.* **2021**, *13*, 1630. <https://doi.org/10.3390/rs13091630>

Academic Editor: Yoshio Inoue

Received: 23 March 2021

Accepted: 18 April 2021

Published: 21 April 2021

Publisher's Note: MDPI stays neutral with regard to jurisdictional claims in published maps and institutional affiliations.



Copyright: © 2021 by the authors. Licensee MDPI, Basel, Switzerland. This article is an open access article distributed under the terms and conditions of the Creative Commons Attribution (CC BY) license (<https://creativecommons.org/licenses/by/4.0/>).

Abstract: With the increase in the frequency of extreme weather events in recent years, apple growing areas in the Loess Plateau frequently encounter frost during flowering. Accurately assessing the frost loss in orchards during the flowering period is of great significance for optimizing disaster prevention measures, market apple price regulation, agricultural insurance, and government subsidy programs. The previous research on orchard frost disasters is mainly focused on early risk warning. Therefore, to effectively quantify orchard frost loss, this paper proposes a frost loss assessment model constructed using meteorological and remote sensing information and applies this model to the regional-scale assessment of orchard fruit loss after frost. As an example, this article examines a frost event that occurred during the apple flowering period in Luochuan County, Northwestern China, on 17 April 2020. A multivariable linear regression (MLR) model was constructed based on the orchard planting years, the number of flowering days, and the chill accumulation before frost, as well as the minimum temperature and daily temperature difference on the day of frost. Then, the model simulation accuracy was verified using the leave-one-out cross-validation (LOOCV) method, and the coefficient of determination (R^2), the root mean square error (RMSE), and the normalized root mean square error (NRMSE) were 0.69, 18.76%, and 18.76%, respectively. Additionally, the extended Fourier amplitude sensitivity test (EFAST) method was used for the sensitivity analysis of the model parameters. The results show that the simulated apple orchard fruit number reduction ratio is highly sensitive to the minimum temperature on the day of frost, and the chill accumulation and planting years before the frost, with sensitivity values of ≥ 0.74 , ≥ 0.25 , and ≥ 0.15 , respectively. This research can not only assist governments in optimizing traditional orchard frost prevention measures and market price regulation but can also provide a reference for agricultural insurance companies to formulate plans for compensation after frost.

Keywords: apple; frost; flowering; meteorological; remote sensing

1. Introduction

With the development of China's apple industry, its apple planting area and output have grown to account for 42.24% and 45.54% of the world's total, respectively, and the country has become the world's largest apple producer in terms of planting area. However, China's apple industry faces the problem of low yield per unit area. China's average apple yield is 18.94 tons/ha, ranking only 31st in the world, behind countries with more developed apple planting industries such as Switzerland (59.11 tons/ha), New Zealand

(53.14 tons/ha), and Chile (50.17 tons/ha) [1]. Therefore, China's apple industry needs to optimize the regional planting structure and further increase the high-quality-fruit output of orchards to improve the current situation of low yield per unit area. The apple cultivation areas with the largest planting area in China are mainly distributed in Shaanxi Province, Shandong Province, Gansu Province, Shanxi Province, Henan Province, and other provinces, and the Fuji variety is the most widely planted [2]. Shaanxi Province, which is located in the Loess Plateau, China's main apple-producing area, has experienced frequent frost disasters during the apple flowering period in recent years, which has caused reduced production or a complete loss of production in a large number of apple orchards [3]. In this context, the accurate estimation of orchard yield loss due to frost at the regional scale can enable government management departments to formulate appropriate orchard management measures such as optimizing the regional planting structure and precise irrigation, fertilization, and pesticide application in a timely manner to improve orchard yield per unit area [4]. Furthermore, it is imperative to understand the mechanism of frost damage during the flowering period of fruit trees to perform orchard loss assessment under the background of frost damage.

The dormancy period of temperate plants consists of three stages, namely endodormancy, ecodormancy, and paradormancy [5]. Frost damage events in apple orchards generally occur in the ecodormancy stage of the dormancy period. The chill accumulation required for plants to break their natural dormancy needs to be exceeded, and then, under the influence of warm temperatures in spring, the plants begin to accumulate heat until they meet the heat demand to resume growth (e.g., budding and flowering). However, in recent years, the spring phenology of perennial vegetation in temperate regions has shown an advancing trend [6–8], which has increased the risk of plants suffering damage from frost weather [9,10]. Studies have shown that plants have cold adaptability, which enables them to survive the low-temperature environment in winter [8]. The cold adaptability of plants is gradually strengthened with the decrease of environmental temperature [8]. If plants are suddenly exposed to frost weather in the spring phenology stage, irreversible damage will be caused to the new tissues of the plants [11]. Some studies have shown that when flower buds bloom, the lethal temperature of the flower's reproductive organs will increase, which is equivalent to the loss of cold tolerance in this part of the plant tissue [12,13].

The assessment of frost risk in orchards can not only assist fruit industry management departments in planning suitable planting areas but can also help guide the design and installation of frost damage prevention systems [12]. Additionally, the effective assessment of frost risk is essential to quantify the loss of orchard yield [10]. Therefore, to ensure the sustainable development of the fruit industry in China, it is urgent to accurately assess the loss of apple orchard yield caused by frost disasters. In the past, the assessment of frost damage to orchards mainly relied on limited manual sampling methods. However, such methods are usually time-consuming and labor-intensive, and the results are easily subject to subjective interpretation by researchers, making them unrepresentative [14]. Moreover, traditional manual sampling methods cannot meet the needs of regional-scale orchard frost damage surveys. The development of remote sensing equipment and information technology has allowed many researchers to assess the frost hazard of various types of vegetation. Previous studies used daily temperature data from the gridded surface meteorological dataset (gridMET) [15] and site observations [12], combined with specific lethal temperature thresholds corresponding to different phenological periods of perennial orchards, to assess the probability of frost disasters at various production sites. Additionally, based on the principle that early germination may increase the ability of trees to adapt to cold environments and late germination may reduce the frost risk, Bennie et al. optimized the parameters of the thermal time bud-burst model by using a birch germination dataset based on field site surveys to evaluate the probability of frost damage to birch trees [16]. However, the lack of hourly temperature data and phenological data often limits the ability to improve the evaluation accuracy of frost damage models. Furthermore, in remote

sensing applications, the abnormal areas in time-series of satellite images can often reflect unexpected changes in vegetation. Therefore, Bascietto et al. developed a machine learning-based method for the automatic detection of beech frost loss based on time-series of EVI satellite images [10]. Studies have also proposed a spring frost damage index (SFDI) based on remote sensing data to quantify the yield loss in winter wheat after frost damage [17]. In apple trees, the distribution of leaves and flowers in the flowering period is relatively sparse. Therefore, after a frost injury event, it is difficult to distinguish frost-damaged apple flowers from normal apple flowers from remote sensing images. Therefore, the degree of frost injury in apple trees at the flowering stage cannot be directly determined from such images.

This study combines remote sensing and meteorological information to assess the impact of frost damage during apple flowering. Since the cold adaptability of plants under natural conditions tends to increase with continuous low-temperature weather, when extreme low-temperature weather occurs suddenly (e.g., frost), the flowers and young buds of plants will be irreversibly damaged. Therefore, in this work, the number of flowering days and chill accumulation before the occurrence of frost injury to apples, as well as the minimum temperature and daily temperature difference on the day of frost injury, were used as meteorological predictors for the assessment of apple loss from frost injury. Additionally, a field investigation was performed, which showed that after the occurrence of a frost event, fruit trees with different planting years often exhibit different degrees of frost damage during the flowering period; therefore, in this study, the apple planting years were used as a predictor for the remote sensing-based evaluation of apple frost damage. This study has combined the advantages of remote sensing and meteorological information to assess the impact of frost damage during the flowering period of apples at the regional scale. The results can provide a reference for insurance companies to formulate insurance claim plans for frost damage during the flowering period.

2. Materials and Methods

2.1. Study Area

In recent years, the apple growing area in the Loess Plateau of Northwestern China has suffered frequent frost damage during the apple flowering period. This study focused on the investigation of frost damage in the main apple producing area in Luochuan County, Shaanxi Province. Luochuan County, which is located in the Loess Plateau region in central Shaanxi (Figure 1), lies in the northern temperate zone and has a continental humid and arid monsoon climate. Additionally, the temperature and precipitation information of Luochuan County was obtained according to the annual ground value data set (1981–2010) of the China National Meteorological Science Data Center (<http://data.cma.cn/site/index.html>, accessed on 6 August 2020). Among them, the annual average rainfall, annual maximum rainfall, and annual minimum rainfall were 592.4 mm, 929.4 mm, and 341.9 mm, respectively. The annual average temperature, annual maximum temperature, and annual minimum temperature were 10 °C, 15.7 °C, and 5.1 °C, respectively. The study area has sufficient sunshine for apple growth, and a large temperature difference between day and night, which is very suitable for the growth of apple trees. In addition to the apple trees planted in this area, other vegetation is present, including low shrubs and evergreen coniferous forests.

2.2. Field Data

Due to an extreme low-temperature event that occurred in the study area on 17 April 2020—during the apple flowering period—a wide range of frosts occurred, which led to a reduced output or a complete loss of output in the apple orchards in the south of Luochuan County. We carried out data collection in 46 apple orchards in Luochuan County in September 2020. The collected data include the number of fruits recorded by apple orchard workers in 2019 (normal year) and 2020 (frost injury year) as well as the corresponding orchard area, tree age, and tree location. Among them, the number of

fruit in the apple orchard recorded in 2019 and 2020 was used to calculate reduction of apple production in the orchards in 2020. The geographic coordinates of the research sites were determined using a Qianxun Position SR2 satellite-based RTK receiver mobile device with a centimeter-level positioning accuracy (Qianxun Spatial Intelligence, Inc., Huzhou, China). Additionally, in order to accurately extract the distribution area of the apple orchard in the study area (the target area for studying frost loss), based on satellite images with decimeter-level spatial resolution in the Google Earth software, we obtained the region of interest (ROI) of training and verification samples for land cover classification in the study area through visual interpretation. This study selected the land cover types in relatively homogeneous areas, including apple orchards (30 samples), coniferous forests (30 samples), grass and shrubs (50 samples), urban (30 samples), bare land (30 samples), and water bodies (10 samples) (see Figure 1).

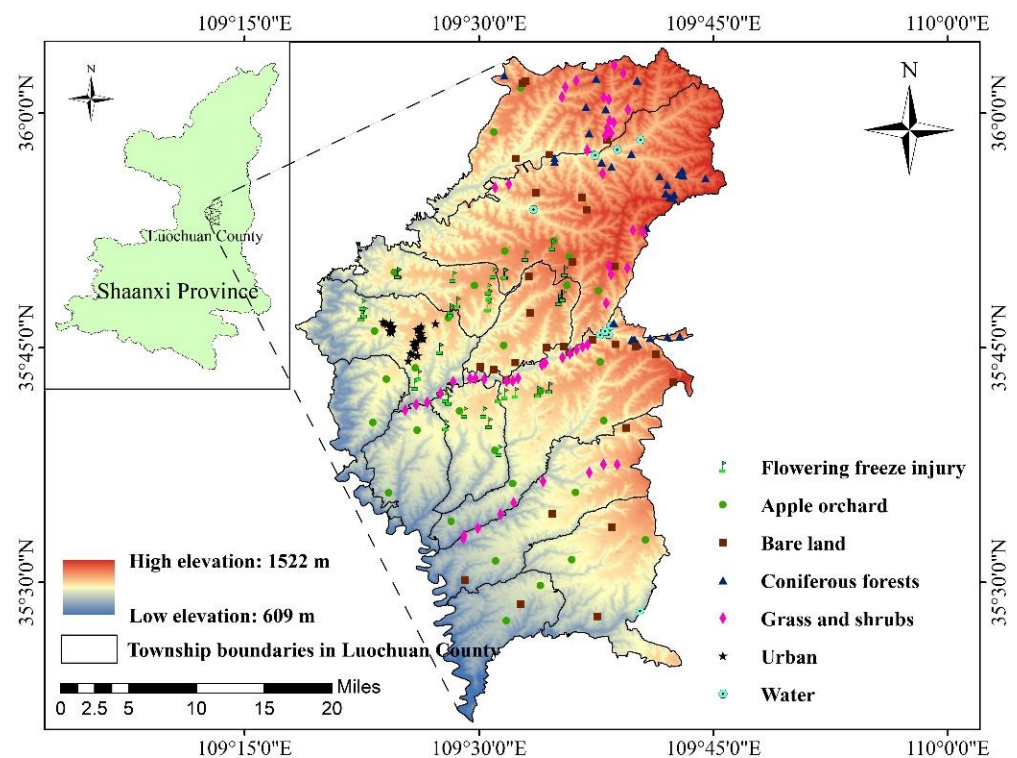


Figure 1. The location of the study area and field samples.

2.3. Remote Sensing and Meteorological Data Acquisition and Preprocessing

This study used the Google Earth Engine (GEE) (<https://code.earthengine.google.com>, accessed on 15 October 2020) to obtain Sentinel-2 and Landsat-TM/ETM+/OLI Normalized Difference Vegetation Index (NDVI) images of the study area. Among them, the Sentinel-2 data were NDVI time-series images of L2A-level surface reflectance products for the 12 months of 2019 (1 scene/month) without clouds or with low cloudiness. The L2A-level data have undergone atmospheric correction, orthorectification, and geometric precision correction for the bottom-of-atmosphere corrected reflectance. Landsat-TM/ETM+/OLI data are an NDVI product synthesized from the 32-day maximum value for cloudless conditions or for cloud cover of less than 5% for June–October from 1990 to 2019. This product can reduce the impact of cloud cover during the study period. Additionally, to compensate for the lack of Landsat images of the corresponding period from 2008 to 2018, this study used Landsat-7 first-level terrain accuracy correction (L1TP) product images for the corresponding period, which were downloaded from the United States Geological Survey (USGS) website, as supplementary data. Considering that the Landsat-7 ETM+ spaceborne scan line corrector (SLC) failed in May 2003, which resulted in missing bands in the obtained images, the “landsat_gapfill.sav” tool in the ENVI 5.3 software (Exelis Visual

Information Solutions, Inc., Boulder, CO, USA) was used to compensate for the missing band data of the images [18].

Additionally, the meteorological data in this paper uses the High-Resolution China Meteorological Administration Land Data Assimilation System (HR-CLDAS) gridded product produced (temporal and spatial resolutions are 1 h and 1 km, respectively) by the China Meteorological Administration, which includes six meteorological parameters: temperature, humidity, rainfall, air pressure, wind speed, and solar short wave radiation. The temperature, air pressure, humidity, and wind speed products are formed based on the multi-grid three-dimensional variational technology and the fusion of ECMWF numerical analysis/forecast products and the observation data of the ground weather automatic station [19]. The actual observation data from more than 2380 national-level automatic meteorological stations was used to evaluate the temperature, air pressure, humidity, and wind speed, and the results showed a good agreement with the actual observations on the ground [20]. According to the developmental stages of apple flowering phenology in the study area, we obtained gridded temperature data from 1 October 2019 to 30 April 2020.

2.4. Method

The advantage of gridded meteorological data is that they can accurately record temperature changes at the regional scale. The advantage of satellite remote sensing images is that they can be used to continuously observe changes in land surface cover. This study combines the advantages of meteorological and remote sensing information to assess apple loss from freeze damage at the regional scale (Figure 2). The following three subsections introduce the detailed implementation steps of this method.

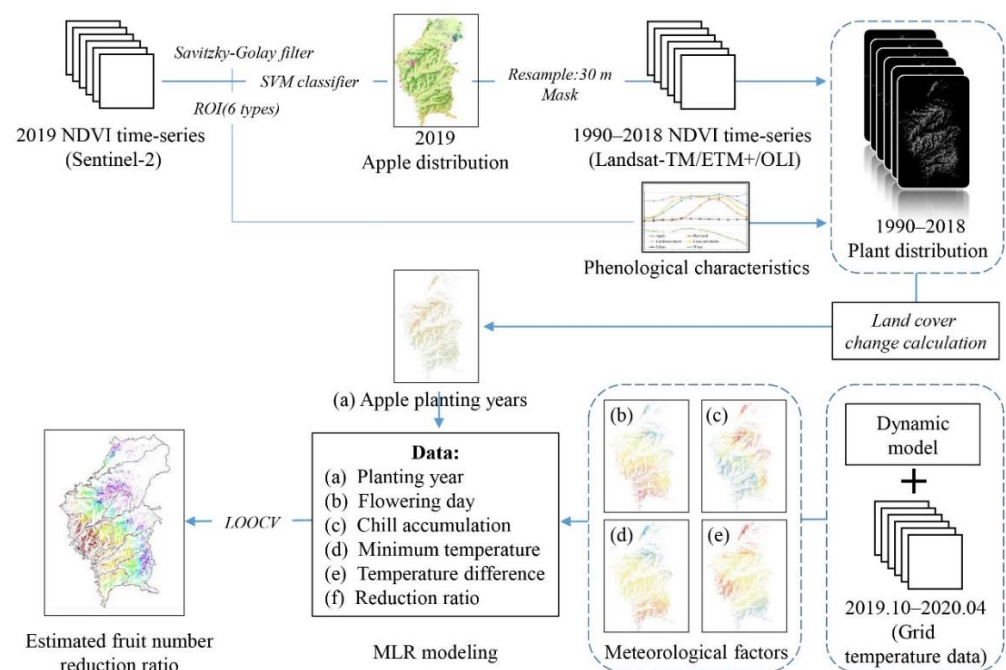


Figure 2. A schematic showing the methodology employed in this study.

2.4.1. Extracting the Planting Years of Apple Orchards Based on Remote Sensing Time-Series Data

In the field survey, it was found that apple trees with different planting years showed some differences in frost damage during flowering. Therefore, the orchard planting years information extracted from the remote sensing time-series data was determined as one of the predictors of orchard freeze damage loss. During the first year of planting, the NDVI values of apple orchards often have the characteristics of bare land. This study draws on a previous method involving the use of remote sensing time-series data combined

with vegetation cover change characteristics to determine the continuous growth years of existing apple orchards [21]—that is, if the distribution area of the existing apple orchard is determined, it is only necessary to determine the change in the distribution area of bare land in this area over time to determine the planting years of the apple trees. The method is mainly divided into three steps. First, determine the distribution area of the existing orchard and use it as the ROI for extracting the apple planting years; then, according to the ROI, mask the remote sensing images each year and use the change characteristics of the NDVI time-series to distinguish the apple orchard distribution in different years; and finally, use the inverse time-series pixel-by-pixel calculation method to obtain the orchard planting years.

In order to effectively extract the distribution of apple orchards in the study area, satellite images with decimeter-level spatial resolution in the Google Earth software were used to obtain the ROI of six different land cover types in the study area, namely apple orchards, coniferous forests, grass and shrubs, cities, bare land, and water bodies. The excellent performance of the support vector machine (SVM) classifier has been shown by many studies [22,23]. In this paper, SVM was used to supervise and classify the NDVI time-series data for the 12 months of 2019. The kernel type, gamma parameter, and penalty coefficient in the SVM classifier were set to the radial basis function, 0.083, and 100, respectively. Then, based on the independent verification samples obtained from the field survey, the confusion matrix verification results were used to test the accuracy of the classification. Finally, the distribution area of apple trees in Luochuan County in 2019 was obtained, and the current apple planting area was used as the ROI for extracting the planting years, that is, the apple planting area was used as a mask file to mask the historical image data. Additionally, based on the Sentinel-2 data, the NDVI time-series of the six land cover types for the 12 months of 2019 were extracted. Given the consistency of the growth relationship between vegetations in different years, the NDVI value representing the growth state index of the vegetation should also be consistent. In this study, the NDVI time-series for the 12 consecutive months in 2019 was used as the standard reference value, and the difference in phenological characteristics between different vegetations was analyzed. Then, the phenological observation period that can most effectively distinguish apple orchard from bare land was selected. Furthermore, the NDVI time-series ratio of apple orchards and bare land in the same month during the best observation period in 2019 was used as a template (Formula (1)). Finally, the average NDVI between the apple orchard and bare land in the corresponding months of each year was used as the segmentation threshold (Formula (2)) between the two in order to eliminate the interference of the bare land area on the extraction of the orchard planting years and thus effectively extract the apple orchard and vegetation distribution area from 1990 to 2018.

$$\frac{2019_Bare_land\ NDVI_i}{2019_Apple_orchard\ NDVI_i} = \frac{k_Bare_land\ NDVI_i}{k_Apple_orchard\ NDVI_i} \quad (1)$$

$$\text{Segmentation threshold} = \frac{k_Bare_land\ NDVI_i + k_Apple_orchard\ NDVI_i}{2} \quad (2)$$

where i represents the month between June and October; k represents the year between 1990 and 2018; and $2019_Bare_land\ NDVI_i$ and $2019_Apple_orchard\ NDVI_i$ represent the average NDVI value of the i -th month based, respectively, on the bare land and apple orchard ROI regions extracted in 2019.

2.4.2. Extracting Information of Apple Orchards Based on Gridded Meteorological Data

When frost occurs during the flowering period of apples, the opened apple flowers will be damaged [9]. The greater the number of flowering days before frost damage occurs, the higher the flowering ratio of fruit trees and the larger the impact of frost damage on apple production; conversely, the lower the number of flowering days before the occurrence of frost damage, the lower the flowering ratio of fruit trees and the smaller the impact of frost damage on apple production. This indicates that the proportion of fruit loss caused by frost damage during apple flowering may have a strong relationship with the number

of flowering days before this damage. Moreover, since the occurrence of frost weather is generally sudden and the cold adaptability of plants under natural conditions tends to increase with increased exposure to low-temperature weather [8], when plants are exposed to frost weather, they tend to have insufficient cold resistance due to the lack of an adaptation process, and the new tissues of the plants will be irreversibly damaged due to the rapid cooling. This indicates that the minimum temperature and daily temperature difference on the day of frost weather may also be related to apple loss. Additionally, compared with other phenological models of the chill accumulation of fruit trees, research shows that a dynamic model can better simulate the chill accumulation of fruit trees [24]. Dynamic models can adequately simulate the change in chill accumulation of fruit trees under the influence of the external environment in the short term before the occurrence of frost injury during flowering.

Based on the above analysis, this study used the number of flowering days and chill accumulation before frost, as well as the minimum temperature and daily temperature difference on the day of frost, as the meteorological predictors for the evaluation of apple frost loss. First, based on the gridded hourly temperature data combined with a dynamic model (Formula (3)) [25], the chill accumulation of apple trees before the frost (17 April 2020) was obtained. The dynamic model calculates the chilling capacity based on the interaction of temperature. Firstly, low temperature promotes the production of intermediate products with chilling capacity, however, these intermediate products will be destroyed when subjected to higher temperatures. Once a certain amount of intermediate product is formed, it is stored as a stable chilling part (CP). Furthermore, the gridded hourly temperature data were also used to obtain the minimum temperature and daily temperature difference on the day of frost. Then, based on the frost occurrence date and the flowering forecast results obtained in a previous study (Yaohui Zhu et al., unpublished manuscript), the number of flowering days before the frost was obtained.

$$\text{Chill accumulation} = \left\{ \sum_{\text{Start}_{\text{DOY}}} \text{CP} \geq \text{Cr} \right\} \quad (3)$$

where Cr represents the chill requirement, CP represents the accumulated chill, and Start_{DOY} represents the start date of chill accumulation.

2.4.3. Construction of Frost Loss Assessment Model and Accuracy Verification

The number of apples in an orchard in the full-fruit period tends to have small inter-annual differences. Therefore, this study calculated the percentage of fruit loss in the orchards in 2020 based on the difference in the number of apples in the orchard in 2019 (normal year) and that in 2020 (frost injury year). Then, based on the fruit reduction rate and the apple planting years at the field survey sampling points, combined with the corresponding number of flowering days and chill accumulation before frost injury, as well as the minimum temperature and daily temperature difference on the day of frost, a multivariable linear regression (MLR) frost injury loss evaluation model was constructed (Formula (4)).

$$y = C + \beta_1 * (\text{planting years}) + \beta_2 * (\text{flowering days}) + \beta_3 * (\text{chill accumulation}) + \beta_4 * (\text{minimum temperature}) + \beta_5 * (\text{temperature difference}) \quad (4)$$

where y represents the reduction rate of the number of apples; β_1 , β_2 , β_3 , β_4 , and β_5 respectively represent the regression coefficient terms of the corresponding parameters; and C represents a constant.

Based on the frost loss assessment model, the apple planting years, the number of flowering days and chill accumulation before frost, and the minimum temperature and daily temperature difference on the day of frost were input into the model. Finally, the regional freeze damage loss was obtained. Additionally, the orchard frost loss data collected in this study are only 33 samples. If the training set and validation set are divided according to the usual proportions for training, then the data available for the training set

are relatively small. However, the leave-one-out cross-validation (LOOCV) [26] is suitable for evaluating the simulation accuracy of the model in scenarios with a small training set, and can make full use of the data. Therefore, LOOCV method was used to verify the validity of the MLR model. In this study, the indicators used to determine the model simulation accuracy were the coefficient of determination (R^2), root mean square error (RMSE), and normalized root mean square error (NRMSE), which are used to evaluate the error between the estimated value and the observed value. As the RMSE cannot effectively measure the acceptable degree of error between the measured and observed values, the NRMSE index was introduced to evaluate the accuracy of the model: NRMSE values between 0 and 10% represent a good simulation accuracy; values between 10 and 20% represent an acceptable simulation accuracy; and values higher than 20% represent an unacceptable simulation accuracy [21].

$$R^2 = \frac{\sum_{t=1}^n (\hat{y}_t - \bar{y})^2}{\sum_{t=1}^n (y_t - \bar{y})^2} \quad (5)$$

$$\text{RMSE} = \sqrt{\frac{\sum_{t=1}^n (\hat{y}_t - y_t)^2}{n}} \quad (6)$$

$$\text{NRMSE} = \frac{\text{RMSE}}{y_{\max} - y_{\min}} \quad (7)$$

where n represents the number of samples, \hat{y}_t represents the model estimated value, y_t represents the observed value, \bar{y} represents the average observed value, y_{\max} represents the maximum observed value, and y_{\min} represents the minimum observed value.

In this paper, in order to determine the direct and indirect influence of the change in each parameter on the model result, the extended Fourier amplitude sensitivity test (EFAST) was applied using the SimLab2.2 software (<https://ec.europa.eu/jrc/en/samo/simlab>, accessed on 20 December 2020) to obtain the first-order or total-order sensitivity index of each parameter to the model result. The EFAST method is based on the Fourier amplitude sensitivity test (FAST) combined with the advantages of the Sobol method to obtain a global sensitivity analysis method based on variance decomposition [27]. Among them, the first-order sensitivity index reflects the direct contribution rate of parameter X_i to the model results, and the total-order sensitivity index includes the sum of the contribution rates of the interaction between the independent parameter X_i and the other parameters to the model result. For the analysis results to be meaningful, the EFAST method requires that the number of randomly and uniformly generated samples should not be less than 65 times the number of parameters.

3. Results

3.1. Extraction of Apple Orchard Planting Distribution

Different types of vegetation have different characteristics of temporal phenological change. Therefore, this paper selected six vegetation types (apple, coniferous forest, grass and shrubs, urban, bare land, water) according to the main land cover types in the study area. Then, using the GEE platform, Sentinel-2 L2A-level NDVI time-series images for the 12 months of 2019 were obtained, and these were then smoothed and filtered using the Savitzky-Golay (S-G) filter in the ENVI 5.3 software (Exelis Visual Information Solutions, Inc., Boulder, CO, USA). The S-G filter can not only ensure that the shape and width of the time-series data are consistent with the original data but also can effectively remove the noise from the data [28].

In order to effectively extract the distribution area of apple orchards in the study area, we analyzed the time-series NDVI change characteristics and differences of six land cover types. The study found that the curves of different vegetation types are different, including different growth periods, dormancy periods, and growth cycles. For example, the NDVI value of coniferous forests is less affected by seasonal changes and maintains a

high level throughout the year; grass and shrubs have the most similar NDVI phenological characteristics to apples, although the NDVI of grass and shrubs is generally higher than that of apples in spring. Additionally, as shown in Figure 3b, from June to October, the NDVI time-series curve of apple orchards is stable, with values above 0.6. From August to September, the NDVI curve of bare land has a rapid upward trend. This may be due to more rainfall during this period, resulting in the growth of some herbaceous and mosses on the surface of bare land, which makes the NDVI of bare land rise rapidly. In a previous study, Zhu et al. (2020) used NDVI time-series data combined with phenological characteristic parameters to classify research areas containing orchards with different species of tree and obtained an improved mapping accuracy [21]. However, in the region that is investigated in the present research (Luochuan County), only apple trees are used as a major economic orchard tree species, while other types of fruit trees are not planted over a large scale; therefore, the county's planting structure is relatively simple. This study was only based on the 2019 Sentinel-2 NDVI time-series data and the training samples (ROI) of the six types of land cover, the apple planting distribution was obtained using the SVM supervised classification method (see Figure 4).

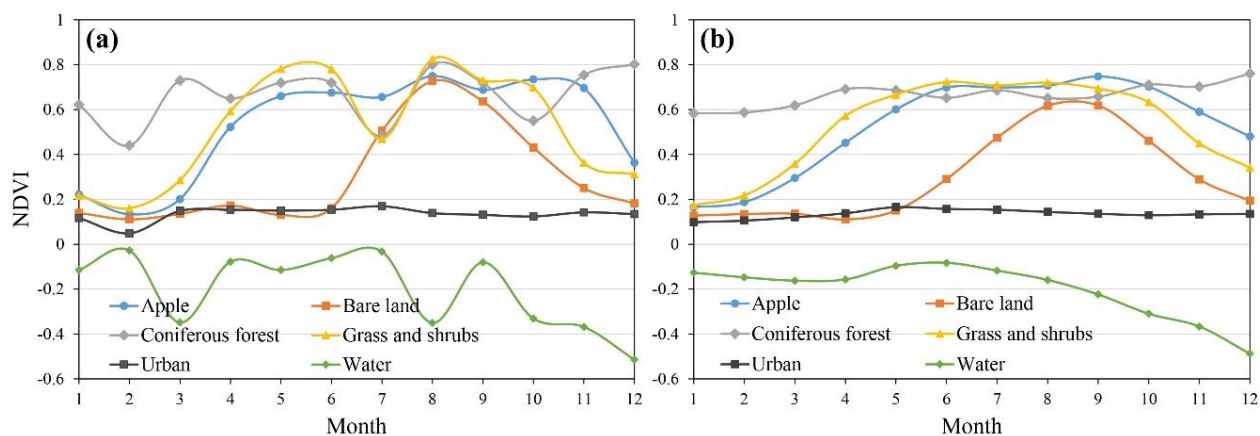


Figure 3. NDVI time-series curves for the main land cover types in Luochuan County in 2020. (a) Original NDVI time-series change curve; (b) NDVI time-series change curve after S-G filtering.

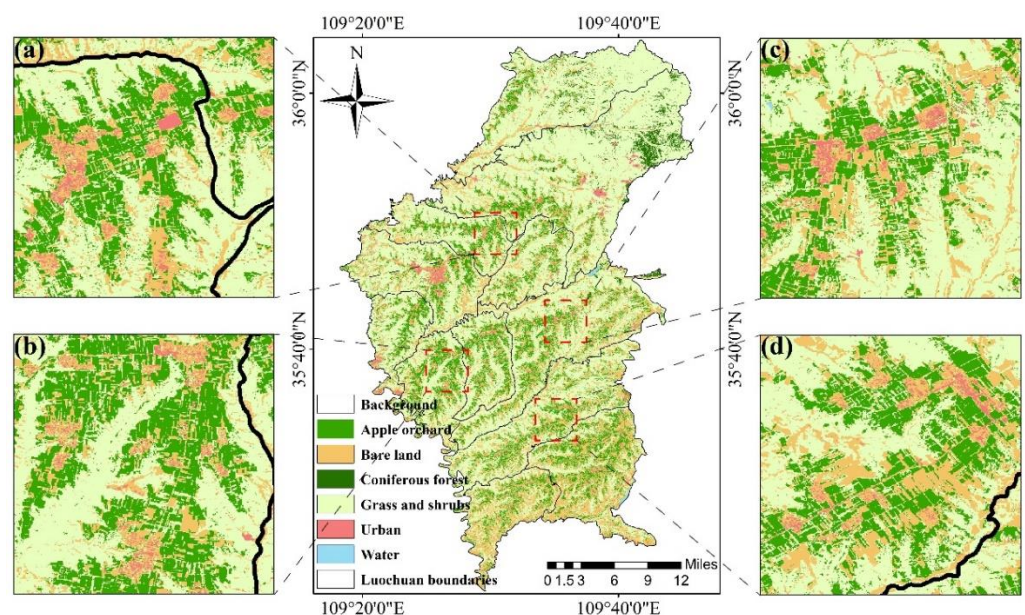


Figure 4. Land coverage classification map. (a–d) show magnifications of the main map.

Then, the confusion matrix verification results based on independent verification samples were used to verify the accuracy of the supervised classification, which included apple orchards (10 samples), bare land (10 samples), coniferous forest (10 samples), grassland shrubs (15 samples), cities (10 samples), and water (10 samples). The confusion matrix verification results (Table 1) show a high overall classification accuracy and Kappa coefficient, reaching 99.38% and 0.99, respectively, and a Producer's Accuracy and User's Accuracy of more than 98.91%. The Producer's Accuracy and User's Accuracy of apple orchard were 98.97% and 98.91%, respectively. For coniferous forest and water, as the annual surface cover change is relatively stable for these land cover types and their NDVI characteristics are quite different from other land cover types (the NDVI of coniferous forest maintains a relatively high value throughout the year, while water has the lowest value throughout the year), the classification accuracy is 100% for both of these two types. The results show that, in this study area with a simple planting structure, using NDVI time-series data throughout the growth cycle can be used to effectively distinguish land cover types.

Table 1. Confusion matrix validation results.

Class	Prod. Acc (%)	User. Acc (%)
Apple Orchard	98.97	98.91
Bare land	100.00	99.66
Coniferous Forest	100.00	100.00
Grass and shrub	99.01	99.16
Urban	99.66	100.00
Water	100.00	100.00
Overall Accuracy	99.38% (5978/6015)	
Kappa coefficient	0.99	

Note: Prod. Acc.: Producer's Accuracy; User. Acc.: User's Accuracy.

3.2. Identification and Verification of Apple Orchard Planting Years

Figure 3 showed that the NDVI value of apple orchard remained stable from June to October, and there was a significant difference between the NDVI value of bare land and the NDVI value of apple orchard. Therefore, the period from June to October was used as a study period to distinguish orchard from bare land, and the NDVI ratio between the orchard and the bare land in different months in this period was calculated as a standard template using Formula 1.

Subsequently, the distribution area of apple orchards in 2019 extracted in Section 3.1 was used as the area of interest to identify the apple orchard planting years, and the NDVI images from 1990 to 2018 were masked separately. Using the apple orchard area with more than 30 years of planting as the area of interest for extracting the average NDVI value, the NDVI images of the corresponding months of each year were input into the apple orchard and bare land ratio (Formula (1)) to obtain the average NDVI value of the bare land. Next, the vegetation distribution area of Luochuan County from 1990 to 2018 was obtained using the segmentation threshold method (Formula (2)). The 10-m resolution apple orchard distribution results obtained after the SVM classification based on the 2019 Sentinel-2 NDVI image time-series were resampled to the resolution of the Landsat image, namely 30 m. Then, based on the 30-m resolution images obtained between 1990 and 2019, the pixel-by-pixel inverse time-series calculation method was used to obtain the apple orchard planting years distribution (see Figure 5).

Field-observed apple orchard planting years data were used to verify the identification results. The results show that the planting years identification results achieved a good accuracy (see Figure 6). The R^2 , RMSE, and NRMSE were 0.82, 4.27 years, and 15.84%, respectively. Additionally, the verification results show that when the planting years exceed 20 years, the planting years are underestimated. Compared to 2000–2019 (contains Landsat-5/7/8 remote sensing images), this may be due to the fact that only Landsat-5 satellite

remote sensing images were obtained from 1990 to 1999, and there are fewer high-quality cloud-free images to choose from.

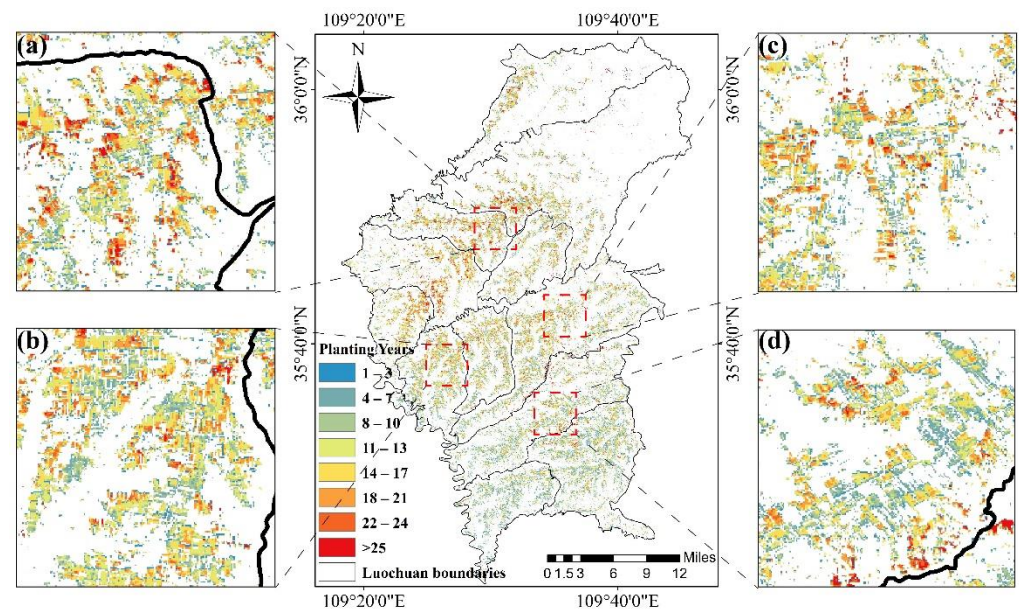


Figure 5. A map showing the distribution of apple orchard planting years in the study area. (a–d) show magnifications of the main map.

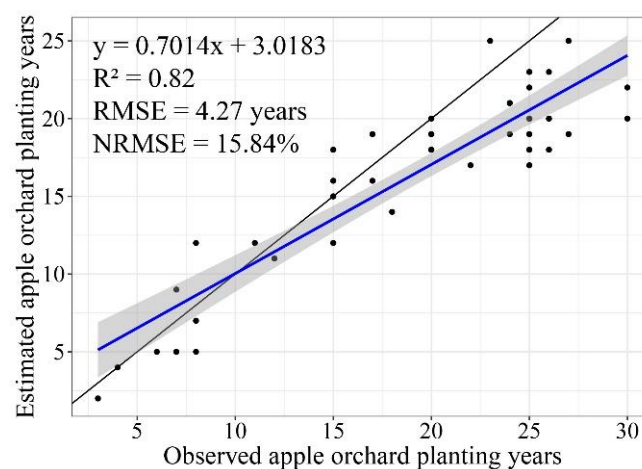


Figure 6. The accuracy verification of the estimated apple orchard planting years. The blue line is the best-fitting straight line and the black line is the 1:1 line.

3.3. Extraction of Meteorologically Derived Parameters Based on Gridded Meteorological Data

According to the flowering time of apple tree in Luochuan County in 2020 predicted by in the previous study (Yaohui Zhu et al., unpublished manuscript), we calculated the number of flowering days before the frost injury (17 April 2020), and the results are shown in Figure 7a. The results showed that the number of flowering days before frost damage gradually increased from the northeast to the southwest of the study area. Additionally, the number of flowering days before frost damage and the altitude distribution of the study area maintained similar gradient distribution characteristics. As the altitude increases, the number of flowering days gradually decreases. This is due to the higher altitude in the northeast region, which has lower spring temperatures than the southwest, so that the flowering time is later. Areas with between 11 and 14 flowering days accounted for 28.43% of the apple distribution area, while areas with more than 15 flowering days accounted

for 34.75% of the apple distribution area; meanwhile, the area where apple trees did not bloom before freezing only accounted for 1.78% of the apple distribution area, mostly distributed in the north of the county. The largest number of flowering days before freezing was observed in the south of the county (27 days), and the apple orchards with the latest flowering did not bloom until the sixth day after the frost damage occurred. Field surveys of apple trees have shown that the period from the opening of the first flower to the withering of the last flower is generally about 15 to 20 days. Therefore, the earlier the flowering period, the greater the proportion of flowering fruit trees before the occurrence of frost damage; it follows that, when extreme low-temperature weather occurs, orchards with higher blooming ratios may often suffer more severe frost damage.

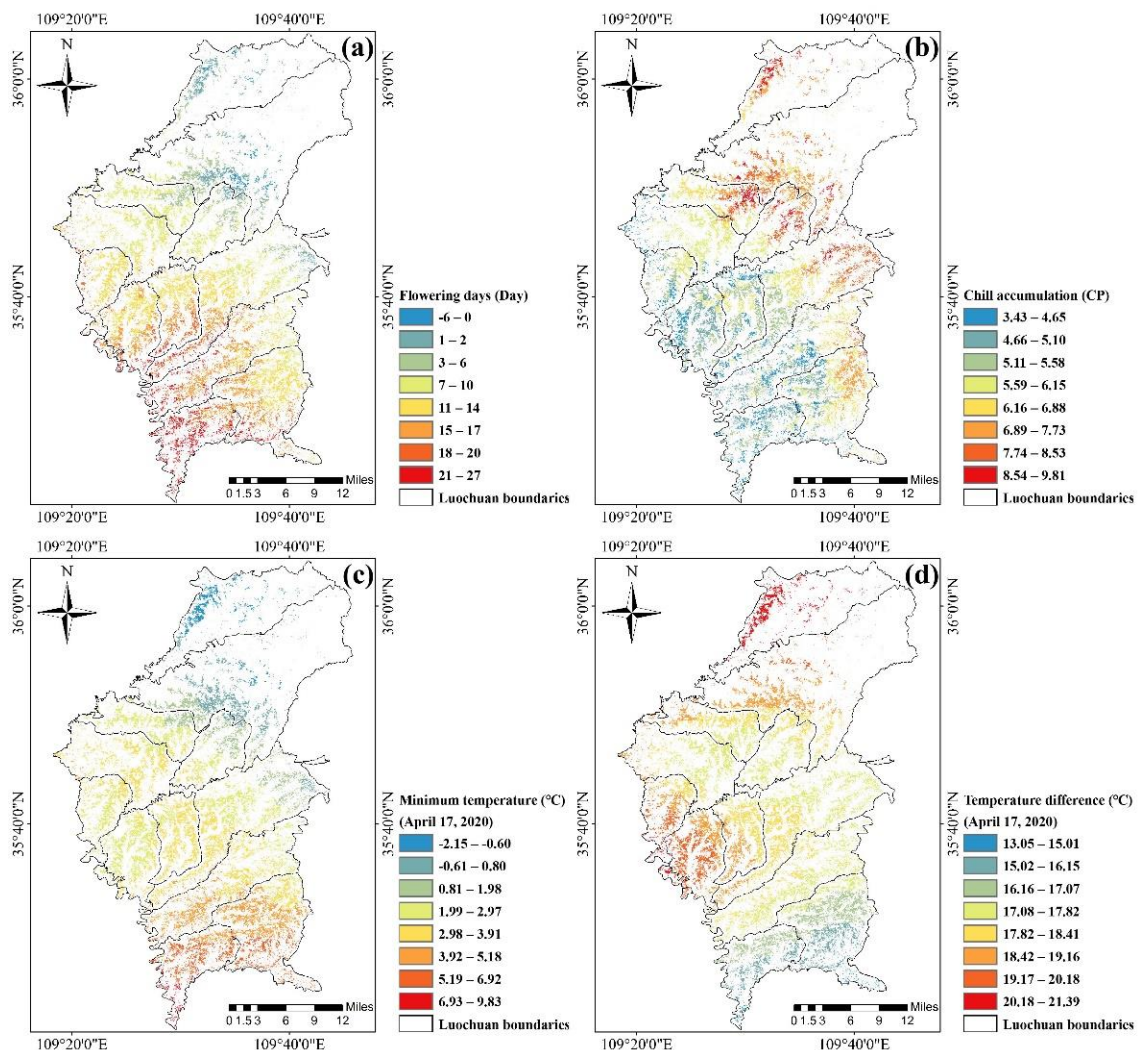


Figure 7. Maps showing the distribution of four meteorologically derived parameters in the study area extracted based on gridded meteorological data. (a) The number of apple flowering days before frost. (b) The chill accumulation between 1 and 17 April 2020 calculated based on gridded meteorological data and the dynamic model. (c) and (d) respectively represent the minimum temperature and daily temperature difference on the day of frost obtained based on gridded meteorological data.

Then, based on the gridded meteorological data and the occurrence time of frost damage during apple flowering, a dynamic model was used to calculate the chill accumulation between 1 and 17 April 2020 (Figure 7b). The results showed that the chill accumulation before frost damage gradually decreases from the northeast to the southwest. Areas with high altitudes have more chill accumulation; on the contrary, areas with low altitudes have less chill accumulation. The area in the southwest of the study area with a chill

accumulation below 6.15 CP accounts for 61.5% of the apple area. The chill accumulation and the number of flowering days before frost injury in the study area showed consistent spatial gradient change trend during this period. Additionally, some previous studies have shown that the arrival of spring phenology (flowering or budding) in fruit trees requires a combination of chill accumulation in winter and heat accumulation in spring to break the dormancy of fruit trees [9,29]. The lower chill accumulation in the southwest of the study area means that fruit trees can receive more heat accumulation and can thus reach the flowering stage earlier. The chill accumulation between 1 and 17 April 2020 can be used to infer the response characteristics of apple trees to environmental temperature changes in the early period of frost damage, which can provide a reference for the estimation of frost damage loss during flowering.

Based on gridded hourly temperature data with a resolution of 1 km for 17 April 2020, this study calculated the minimum temperature (Figure 7c) and daily temperature difference (Figure 7d) for this day. The results show that the minimum temperature on the day of frost gradually decreases from the south to the north of the study area, and the spatial distribution of the minimum temperature gradually decreases with the increase of latitude, but there is no obvious gradient distribution in the longitude (Figure 7c). The spatial distribution of the daily temperature difference gradually increases with the increase of latitude. However, the daily temperature difference in some areas ($35^{\circ}35'$ to $35^{\circ}45'$ N, $109^{\circ}20'$ to $109^{\circ}30'$ E) of the study area has obvious characteristics of aggregation, and the daily temperature difference here is about 2°C higher than other areas of the same latitude (Figure 7d). Previous studies have shown that the low-temperature adaptability of plants gradually increases as they are exposed to low-temperature conditions in the natural environment. However, when plants suddenly experience extreme cold weather (e.g., frost), this may cause damage to plant tissues due to the lack of a low-temperature adaptation process [8]. Therefore, the minimum temperature and daily temperature difference on the day of frost damage can be used to determine the loss of orchard production caused by frost damage during flowering.

3.4. Assessment of Fruit Amount Reduction Ratio Due to Frost during Apple Flowering

Then, an MLR model was constructed based on the apple planting years, the number of flowering days and chill accumulation before frost, the minimum temperature and daily temperature difference on the day of frost, and the fruit amount reduction rate at the positions of the 33 field survey sample points. Finally, based on the obtained regional dataset of the apple orchard planting years, the number of flowering days and chill accumulation before frost, and the minimum temperature and the daily temperature difference on the day of frost, combined with the MLR prediction model for the fruit amount reduction ratio, a distribution map of the regional fruit reduction rate was obtained, as shown in Figure 8. Some values greater than 100% are included in the distribution map, which represent areas where the frost disaster occurred during the flowering period and the fruit amount in the orchard was completely reduced; these values were all set to 100%. Additionally, the map also contains values less than 0%, which means that the amount of fruit in the orchard was not lower in 2020 compared to 2019; similarly, these values were all set to 0%.

From Figure 8, it can be seen that the frost damage was more severe in the west of the county than in the east and the proportion of fruit loss gradually increases from east to west. The area north of $35^{\circ}50'$ N latitude was unaffected or only slightly affected by frost damage, whereas most areas south of $35^{\circ}50'$ N latitude were more seriously affected. Especially in parts of the southwest ($35^{\circ}35'$ to $35^{\circ}45'$ N, $109^{\circ}20'$ to $109^{\circ}30'$ E), the loss of frost in orchards was more serious, and the fruit reduction rate reached more than 90%, which has an obvious aggregation effect in spatial distribution. Considering that the number of flowering days before the frost in this area with severe frost loss reached 11 to 17 days, the flowering state of most orchards was already in full bloom. In addition, compared with other regions, the minimum temperature on the day of the frost in this severe frost loss area

was only 1.99 to 3.91 °C, but the daily temperature difference reached 18.42 to 20.18 °C. Therefore, such a low temperature and large daily temperature difference lead to more serious fruit frost loss in the orchard in full bloom period. Areas with a reduction ratio of >90.0% accounted for 18.6% of the total apple planting area of the study region, and only 9.2% of the apple planting area had no frost damage or slight frost damage (reduction ratio of ≤10.0%).

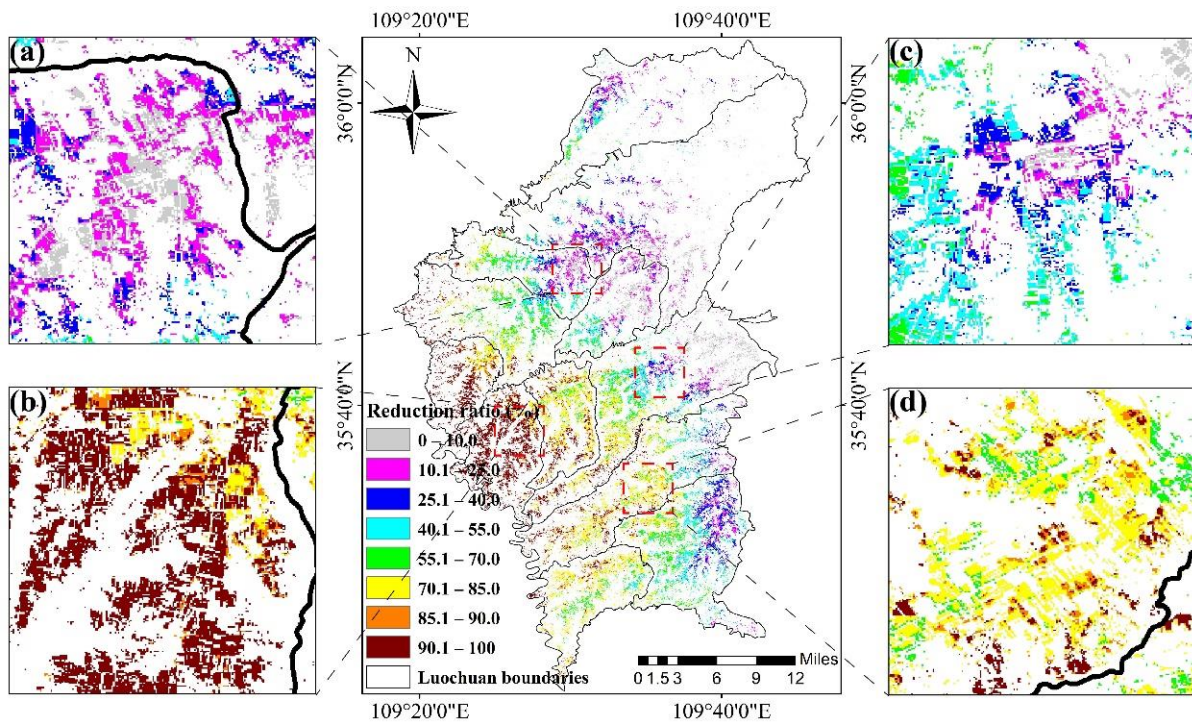


Figure 8. Maps showing the percentage reduction in the number of apples after frost injury in 2020 obtained by the MLR analysis of orchard planting years, the number of flowering days before frost, the chill accumulation before frost, and the minimum temperature and the daily temperature difference on the day of frost. (a–d) are magnifications of the main map.

Furthermore, the results of the LOOCV analysis showed a good modeling and verification accuracy (see Figure 9): the MLR modeling achieved R^2 , RMSE, and NRMSE values of 0.77, 16.06%, and 16.06%, respectively, while the LOOCV obtained R^2 , RMSE, and NRMSE values of 0.69, 18.76%, and 18.76%, respectively.

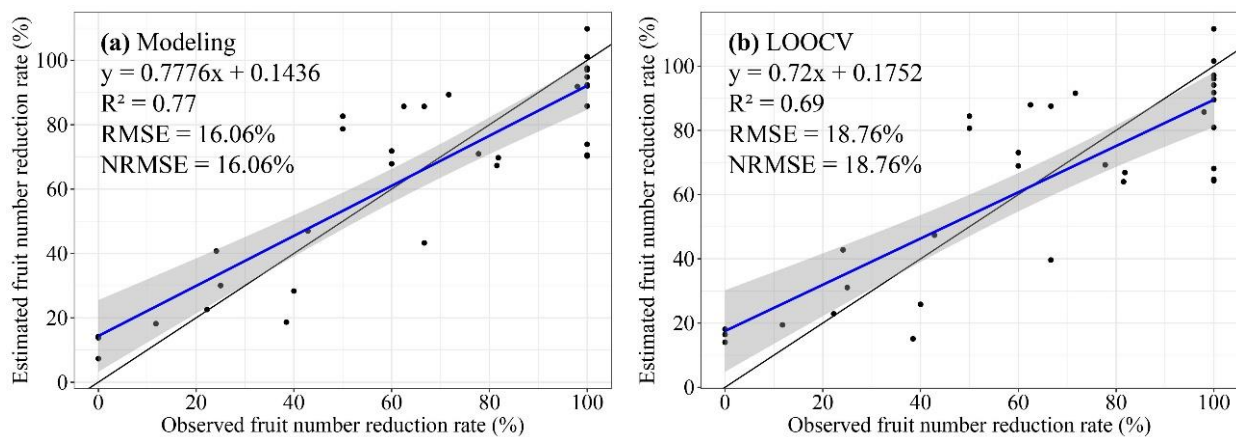


Figure 9. The results of MLR modeling and leave-one-out cross-validation (LOOCV). The blue lines are the best-fitting straight lines and the black lines are the 1:1 lines.

4. Discussion

4.1. Evaluation of the Influence of Meteorological and Remote Sensing Factors in the MLR Model

To test the importance of the five parameters of planting years, the number of flowering days and chill accumulation before frost, and the daily minimum temperature and temperature difference on the day of frost, this paper used the SimLab2.2 tool for parameter sensitivity analysis. The range of sensitivity values of each parameter was determined according to the maximum and minimum values of the corresponding sampling points. The 400 datasets generated for the five prediction parameters were input into the fruit reduction rate evaluation model, and 400 simulated reduction rates were thereby obtained. Then, the simulated parameter dataset and fruit number reduction rates were input into SimLab2.2, and the sensitivity results corresponding to the five parameters were thus obtained (see Table 2).

Table 2. The results of the parameter sensitivity analysis of the MLR model obtained using the SimLab2.2 software.

Parameters	Range (400 Samples)	First-Order Sensitivity Index	Total-Order Sensitivity Index
Planting years	2–25	0.15 (10.86%)	0.17 (11.62%)
Flowering days	1–18	0.12 (8.78%)	0.14 (9.45%)
Chill accumulation	3.8–8.2	0.25 (18.45%)	0.27 (18.50%)
Minimum temperature	0.2–3.8	0.74 (54.19%)	0.75 (52.15%)
Daily temperature difference	17.2–18.6	0.10 (7.72%)	0.12 (8.28%)

Note: The first-order sensitivity index reflects the direct contribution rate of parameter X_i to the model results, and the total-order sensitivity index includes the sum of the contribution rate of the interaction between the independent parameter X_i and other parameters to the model result. The percentages in parentheses represent the parameter's contribution to the sensitivity index.

The results in Table 2 show that, regardless of whether the influence of the parameters on the prediction results was considered independently (first-order sensitivity index) or comprehensively (total-order sensitivity index), a consistent parameter sensitivity order was obtained: minimum temperature > chill accumulation > planting year > flowering days > daily temperature difference. That is, the fruit amount reduction rate is most sensitive to the minimum temperature on the day of frost, with sensitivity indices ≥ 0.74 . The parameter with the second-highest sensitivity index is the chill accumulation before frost, with sensitivity indices ≥ 0.25 . The sum of the contribution rates of the minimum temperature, chill accumulation, and planting year accounts for more than 82% of the result, which indicates that these three parameters should be taken as the main model parameters in future assessments of orchard frost loss. It is worth noting that the simulated fruit reduction rate is more sensitive to the planting years (first-order and total sensitivity indices of 0.15 and 0.17, respectively) than the number of flowering days and the daily temperature difference. This shows that planting year information (obtained based on remote-sensing data) is effective for the assessment of frost disasters in apple orchards and has potential for use in future applications.

4.2. Frost Loss Assessment of Apple Orchard under the Background of Frost Injury

The accurate estimation of frost losses in orchards is essential for optimizing orchard management strategies, disaster assessment, procurement planning, and logistics and transportation. Research on frost risk assessment in orchards has been widely reported and has included studies of the impact of frost on the future distribution of grape planting in Europe [30], as well as the spring frost risk assessment of fruit trees in southern Patagonia [12], orchards in California [15], and high-altitude areas in Switzerland [13]. Researchers have also used remote sensing technology to estimate the damage to winter wheat caused by spring frost based on the difference in the vegetation index of winter wheat before and after the spring frost to assess the degree of damage [17]. However, the leaves and flowers of apple trees are relatively sparse in the flowering period. After frost, it is difficult to

effectively identify frost damage to apple flowers based on satellite remote sensing images. In recent years, with the development of the agricultural insurance industry, the demand for agricultural frost damage assessment has become more and more urgent. However, the goal of most studies tends to be frost damage risk assessment, whereas there are few reports on the assessment of frost loss in orchards.

In field investigations, researchers have found that the degree of frost loss of apples is related to the orchard planting years, the number of flowering days before frost, and the minimum temperature and daily temperature difference on the day of frost. In the present study, to consider the influence of external environmental factors on fruit trees, the element of the chill accumulation of fruit trees in the early stage of flowering was added to the model. Therefore, to solve the limitations of the estimation of frost loss in orchards at a regional scale, this article combines remote sensing and meteorologically derived information based on previous research [21] (Yaohui Zhu et al., unpublished manuscript). This paper proposes a method based on the remote sensing-based extraction of orchard planting years, and the meteorological data-based extraction of the number of fruit tree flowering days and chill accumulation before frost and the minimum temperature and daily temperature difference on the day of frost damage, which, combined with field survey data of orchard yield loss, is used to construct a frost damage loss assessment model.

4.3. Application Prospects for the Assessment of Fruit Amount Loss Based on Frost Injury Analysis

Traditional assessments of orchard frost loss are often obtained by comparing the number of fruits in the current year and previous years by means of field surveys. However, manual survey methods are time-consuming and laborious and are difficult to generalize to regional scales [31]. Therefore, this research proposes a method combining remote sensing and meteorologically derived information to quickly assess fruit loss in orchards due to frost damage. Accurately assessing the proportion of orchard production reduction due to frost damage at a regional scale is of great significance for optimizing water and fertilizer management, planting planning, product processing, and sales programs of orchards [12,13,15,32]. This can effectively promote the reform of the traditional development layout of the fruit industry and further guide management departments of the government fruit industry to formulate market supply plans [14] and price control [33] as well as improve the stability of market operations and consumer satisfaction. Therefore, timely access to regional orchard frost loss information has wide-ranging impacts on governments, enterprises, farmers, and consumers.

Additionally, during the flowering period of apples, the flowers and buds of the fruit trees are extremely vulnerable to frost, which often results in a significant reduction in the amount of fruit in the orchard or may even cause no fruit to be harvested. The associated economic losses can be devastating to farmers. In the process of agricultural development, the agricultural insurance system is playing an increasingly important role in disaster risk management [34]. After an orchard suffers frost damage during the flowering period, accurate and efficient orchard loss estimation is conducive to the rapid implementation of insurance claims by insurance companies, which not only speeds up the payment of farmers' economic losses but also reduces the insurance company's manpower input and expenses.

5. Conclusions

This research proposes an orchard frost loss assessment method using meteorologically derived information (the number of flowering days and chill accumulation before frost and the minimum temperature and daily temperature difference on the day of frost) and remote sensing-derived information (apple orchard planting year), combined with data from field investigations of the orchard fruit number reduction ratio. The verification results show that the simulation accuracy of fruit reduction rate in the orchard is good, and its R², RMSE and NRMSE reach 0.69, 18.76% and 18.76% respectively. Additionally, the SimLab2.2 tool was used to evaluate the sensitivity of the simulation results to the model

parameters. The results showed that, for both the first-order and total-order sensitivity index, the sum of the contribution rates of the minimum temperature, chill accumulation, and planting year accounts for more than 82% of the result. Therefore, it is recommended that these three parameters should be considered as the main model parameters when assessing the frost loss of apple orchards in the future. In the future, after frost disaster occurs during the flowering period in Luochuan County, this research can not only guide the government to formulate market supply and price control plans but can also provide references for insurance companies to formulate insurance claims plans. Additionally, the frost loss evaluation model that is planned to be established in a follow-up study will further consider the differences in apple varieties in the study area, which will potentially allow the frost loss evaluation method to be extended to other regions.

Author Contributions: Conceptualization, Y.Z.; data curation, Y.Z. and H.Y.; investigation, Y.Z., C.Z. (Chengjian Zhang), J.C. and S.H.; methodology, Y.Z., G.Y. and H.Y.; project administration, G.Y.; resources, G.Y.; software, Y.Z., F.Z. and R.C.; supervision, G.Y.; validation, Y.Z., M.L. and X.Y.; visualization, Y.Z.; writing—original draft, Y.Z.; writing—review & editing, G.Y. and C.Z. (Chunjiang Zhao). All authors have read and agreed to the published version of the manuscript.

Funding: This study was supported by the Key-Area Research and Development Program of Guangdong Province (2019B020216001, 2019B020214002), the National Key Research and Development Program of China (2017YFE0122500).

Institutional Review Board Statement: Not applicable.

Informed Consent Statement: Not applicable.

Data Availability Statement: This study used the Google Earth Engine (<https://code.earthengine.google.com>, accessed on 15 October 2020) to obtain Sentinel-2 and Landsat-TM/ETM+/OLI Normalized Difference Vegetation Index (NDVI) images of the study area. The meteorological data in this paper uses the High-Resolution China Meteorological Administration Land Data Assimilation System (HR-CLDAS) gridded product produced (<http://data.cma.cn/site/index.html>, accessed on 6 August 2020).

Conflicts of Interest: The authors declare no conflict of interest.

References

1. FAO (Food and Agriculture Organization of the United Nations). FAOSTAT Production Database. FAO, 2018. Available online: <http://www.fao.org/faostat/zh/#data/QC> (accessed on 5 December 2020).
2. Wang, N.; Wolf, J.; Zhang, F.-S. Towards sustainable intensification of apple production in China—Yield gaps and nutrient use efficiency in apple farming systems. *J. Integr. Agric.* **2016**, *15*, 716–725. [[CrossRef](#)]
3. Qiu, M.J.; Liu, B.C.; Liu, Y.; Wang, K.Y.; Pang, J.Y.; Zhang, X.N.; He, J.N. Simulation of first flowering date for apple and risk assessment of late frost in main producing areas of northern China. *Trans. Chin. Soc. Agric. Eng.* **2020**, *36*, 154–163. [[CrossRef](#)]
4. Cilia, C.; Panigada, C.; Rossini, M.; Meroni, M.; Busetto, L.; Amaducci, S.; Boschetti, M.; Picchi, V.; Colombo, R. Nitrogen Status Assessment for Variable Rate Fertilization in Maize through Hyperspectral Imagery. *Remote Sens.* **2014**, *6*, 6549–6565. [[CrossRef](#)]
5. Guillamón, J.G.; Prudencio, Á.S.; Yuste, J.E.; Dicenta, F.; Sánchez-Pérez, R. Ascorbic acid and prunasin, two candidate biomarkers for endodormancy release in almond flower buds identified by a nontargeted metabolomic study. *Hortic. Res.* **2020**, *7*, 203. [[CrossRef](#)]
6. Piao, S.L.; Liu, Q.; Chen, A.P.; Janssens, I.A.; Fu, Y.S.; Dai, J.H.; Liu, L.L.; Lian, X.; Shen, M.G.; Zhu, X.L. Plant phenology and global climate change: Current progresses and challenges. *Glob. Chang. Biol.* **2019**, *25*, 1922–1940. [[CrossRef](#)] [[PubMed](#)]
7. Ge, Q.S.; Wang, H.J.; Rutishauser, T.; Dai, J.H. Phenological response to climate change in China: A meta-analysis. *Glob. Chang. Biol.* **2015**, *21*, 265–274. [[CrossRef](#)] [[PubMed](#)]
8. Wang, H.J.; Wu, C.Y.; Ciais, P.; Penuelas, J.; Dai, J.H.; Fu, Y.S.; Ge, Q.S. Overestimation of the effect of climatic warming on spring phenology due to misrepresentation of chilling. *Nat. Commun.* **2020**, *11*, 1–9. [[CrossRef](#)]
9. Guo, L.; Wang, J.H.; Li, M.J.; Liu, L.; Xu, J.C.; Cheng, J.M.; Gang, C.C.; Yu, Q.; Chen, J.; Peng, C.H.; et al. Distribution margins as natural laboratories to infer species' flowering responses to climate warming and implications for frost risk. *Agric. For. Meteorol.* **2019**, *268*, 299–307. [[CrossRef](#)]
10. Bascietto, M.; Bajocco, S.; Mazzenga, F.; Matteucci, G. Assessing spring frost effects on beech forests in Central Apennines from remotely-sensed data. *Agric. For. Meteorol.* **2018**, *248*, 240–250. [[CrossRef](#)]
11. Driessche, R.V.D. Survival of coastal and interior Douglas fir seedlings after storage at different temperatures, and effectiveness of cold storage in satisfying chilling requirements. *Can. J. For. Res.* **1977**, *7*, 125–131. [[CrossRef](#)]

12. Cittadini, E.D.; de Ridder, N.; Peri, P.L.; van Keulen, H. A method for assessing frost damage risk in sweet cherry orchards of South Patagonia. *Agric. For. Meteorol.* **2006**, *141*, 235–243. [[CrossRef](#)]
13. Vitasse, Y.; Schneider, L.; Rixen, C.; Christen, D.; Rebetez, M. Increase in the risk of exposure of forest and fruit trees to spring frosts at higher elevations in Switzerland over the last four decades. *Agric. For. Meteorol.* **2018**, *248*, 60–69. [[CrossRef](#)]
14. Sarron, J.; Malezieux, E.; Sane, C.A.B.; Faye, E. Mango Yield Mapping at the Orchard Scale Based on Tree Structure and Land Cover Assessed by UAV. *Remote Sens.* **2018**, *10*, 1900. [[CrossRef](#)]
15. Parker, L.; Pathak, T.; Ostoja, S. Climate change reduces frost exposure for high-value California orchard crops. *Sci. Total Environ.* **2021**, *762*, 143971. [[CrossRef](#)]
16. Bennie, J.; Kubin, E.; Wiltshire, A.; Huntley, B.; Baxter, R. Predicting spatial and temporal patterns of bud-burst and spring frost risk in north-west Europe: The implications of local adaptation to climate. *Glob. Chang. Biol.* **2010**, *16*, 1503–1514. [[CrossRef](#)]
17. Wang, S.; Chen, J.; Rao, Y.H.; Liu, L.C.; Wang, W.Q.; Dong, Q. Response of winter wheat to spring frost from a remote sensing perspective: Damage estimation and influential factors. *ISPRS J. Photogramm. Remote Sens.* **2020**, *168*, 221–235. [[CrossRef](#)]
18. Abd Razak, J.A.B.; Shariff, A.R.B.; bin Ahmad, N.; Sameen, M.I. Mapping rubber trees based on phenological analysis of Landsat time series data-sets. *Geocarto Int.* **2018**, *33*, 627–650. [[CrossRef](#)]
19. Shi, C.X.; Pan, Y.; Gu, J.X.; Xu, B.; Han, S.; Zhu, Z.; Zhang, L.; Sun, S.; Jiang, Z.W. A review of multi-source meteorological data fusion products. *Acta Meteorol. Sin.* **2019**, *77*, 774–783. [[CrossRef](#)]
20. Han, S.; Shi, C.X.; Jiang, Z.W.; Xu, B.; Li, X.F.; Zhang, T.; Jiang, L.P.; Liang, X.; Zhu, Z.; Liu, J.J.; et al. Development and progress of high resolution CMA land surface data assimilation system. *Adv. Meteorol. Sci. Technol.* **2018**, *8*, 102–108. [[CrossRef](#)]
21. Zhu, Y.H.; Yang, G.J.; Yang, H.; Wu, J.T.; Lei, L.; Zhao, F.; Fan, L.L.; Zhao, C.J. Identification of Apple Orchard Planting Year Based on Spatiotemporally Fused Satellite Images and Clustering Analysis of Foliage Phenophase. *Remote Sens.* **2020**, *12*, 1199. [[CrossRef](#)]
22. Geiss, C.; Pelizari, P.A.; Blickensdorfer, L.; Taubenbock, H. Virtual Support Vector Machines with self-learning strategy for classification of multispectral remote sensing imagery. *ISPRS J. Photogramm. Remote Sens.* **2019**, *151*, 42–58. [[CrossRef](#)]
23. Kong, F.J.; Li, X.B.; Wang, H.; Xie, D.F.; Li, X.; Bai, Y.X. Land Cover Classification Based on Fused Data from GF-1 and MODIS NDVI Time Series. *Remote Sens.* **2016**, *8*, 741. [[CrossRef](#)]
24. Fernandez, E.; Whitney, C.; Luedeling, E. The importance of chill model selection—A multi-site analysis. *Eur. J. Agron.* **2020**, *119*, 126103. [[CrossRef](#)]
25. Fishman, S.; Erez, A.; Couvillon, G.A. The temperature dependence of dormancy breaking in plants: Mathematical analysis of a two-step model involving a cooperative transition. *J. Theor. Biol.* **1987**, *124*, 473–483. [[CrossRef](#)]
26. Kearns, M.; Ron, D. Algorithmic Stability and Sanity-Check Bounds for Leave-One-Out Cross-Validation. *Neural Comput.* **1999**, *11*, 1427–1453. [[CrossRef](#)]
27. Saltelli, A.; Tarantola, S.; Chan, K.P.S. A Quantitative Model-Independent Method for Global Sensitivity Analysis of Model Output. *Technometrics* **1999**, *41*, 39–56. [[CrossRef](#)]
28. Shao, Y.; Lunetta, R.S.; Wheeler, B.; Iiames, J.S.; Campbell, J.B. An evaluation of time-series smoothing algorithms for land-cover classifications using MODIS-NDVI multi-temporal data. *Remote Sens. Environ.* **2016**, *174*, 258–265. [[CrossRef](#)]
29. Guo, L.; Dai, J.H.; Wang, M.C.; Xu, J.C.; Luedeling, E. Responses of spring phenology in temperate zone trees to climate warming: A case study of apricot flowering in China. *Agric. For. Meteorol.* **2015**, *201*, 1–7. [[CrossRef](#)]
30. Leolini, L.; Moriondo, M.; Fila, G.; Costafreda-Aumedes, S.; Ferrise, R.; Bindi, M. Late spring frost impacts on future grapevine distribution in Europe. *Field Crop. Res.* **2018**, *222*, 197–208. [[CrossRef](#)]
31. Di Gennaro, S.F.; Toscano, P.; Cinat, P.; Berton, A.; Matese, A. A Low-Cost and Unsupervised Image Recognition Methodology for Yield Estimation in a Vineyard. *Front. Plant Sci.* **2019**, *10*, 559. [[CrossRef](#)]
32. Bai, T.C.; Wang, S.G.; Meng, W.B.; Zhang, N.N.; Wang, T.; Chen, Y.Q.; Mercatoris, B. Assimilation of Remotely-Sensed LAI into WOFOST Model with the SUBPLEX Algorithm for Improving the Field-Scale Jujube Yield Forecasts. *Remote Sens.* **2019**, *11*, 1945. [[CrossRef](#)]
33. Zhang, Z.; Jin, Y.F.; Chen, B.; Brown, P. California Almond Yield Prediction at the Orchard Level With a Machine Learning Approach. *Front. Plant Sci.* **2019**, *10*, 809. [[CrossRef](#)] [[PubMed](#)]
34. Miranda, C.; Santesteban, L.G.; Urrestarazu, J.; Loidi, M.; Royo, J.B. Sampling Stratification Using Aerial Imagery to Estimate Fruit Load in Peach Tree Orchards. *Agriculture* **2018**, *8*, 78. [[CrossRef](#)]